

RESEARCH ARTICLE

10.1002/2016JG003580

Key Points:

- We examined how environmental conditions affect the relationship between remotely sensed solar-induced fluorescence and photosynthesis
- The relationship appeared robust even under high light and stress conditions although some nonlinearity was noticed
- Solar-induced fluorescence provided very weak constraints on V_{cmax} estimates

Supporting Information:

- Supporting Information S1

Correspondence to:

M. Verma,
manishve@umich.edu

Citation:

Verma, M., et al. (2017), Effect of environmental conditions on the relationship between solar-induced fluorescence and gross primary productivity at an OzFlux grassland site, *J. Geophys. Res. Biogeosci.*, 122, 716–733, doi:10.1002/2016JG003580.



Received 11 AUG 2016

Accepted 15 MAR 2017

Accepted article online 17 MAR 2017

Published online 30 MAR 2017

Effect of environmental conditions on the relationship between solar-induced fluorescence and gross primary productivity at an OzFlux grassland site

Manish Verma^{1,2}, David Schimel¹, Bradley Evans³, Christian Frankenberg^{1,4} , Jason Beringer⁵ , Darren T. Drewry¹, Troy Magney¹, Ian Marang³, Lindsay Hutley⁶, Caitlin Moore⁷, and Annmarie Eldering¹

¹Jet Propulsion Laboratory, California Institute of Technology, Pasadena, California, USA, ²Consulting for Statistics, Computing and Analytics Research, University of Michigan, Ann Arbor, Michigan, USA, ³Faculty of Agriculture and Environment, School of Life and Environmental Sciences, University of Sydney, Sydney, New South Wales, Australia, ⁴Division of Geological and Planetary Sciences, California Institute of Technology, Pasadena, California, USA, ⁵School of Earth and Environment, University of Western Australia, Crawley, Western Australia, Australia, ⁶School of Environment, Charles Darwin University, Darwin, Northern Territory, Australia, ⁷School of Earth, Atmosphere and Environment, Monash University, Melbourne, Victoria, Australia

Abstract Recent studies have utilized coarse spatial and temporal resolution remotely sensed solar-induced fluorescence (SIF) for modeling terrestrial gross primary productivity (GPP) at regional scales. Although these studies have demonstrated the potential of SIF, there have been concerns about the ecophysiological basis of the relationship between SIF and GPP in different environmental conditions. Launched in 2014, the Orbiting Carbon Observatory-2 (OCO-2) has enabled fine-scale (1.3 by 2.5 km) retrievals of SIF that are comparable with measurements recorded at eddy covariance towers. In this study, we examine the effect of environmental conditions on the relationship of OCO-2 SIF with tower GPP over the course of a growing season at a well-characterized natural grassland site. Combining OCO-2 SIF and eddy covariance tower data with a canopy radiative transfer and an ecosystem model, we also assess the potential of OCO-2 SIF to constrain the estimates of V_{cmax} , one of the most important parameters in ecosystem models. Based on the results, we suggest that although environmental conditions play a role in determining the nature of relationship between SIF and GPP, overall, the linear relationship is more robust at ecosystem scale than the theory based on leaf-level processes might suggest. Our study also shows that the ability of SIF to constrain V_{cmax} is weak at the selected site.

1. Introduction

Terrestrial gross primary productivity (GPP) drives the terrestrial food chain and is the largest component of the global carbon cycle. It also displays large spatial and temporal variability at different scales [Heimann and Reichstein, 2008] and can dampen or amplify perturbations to the climate system. Understanding and quantifying spatiotemporal variation in GPP is thus important for monitoring food security, the global carbon cycle, and the climate system [Schimel et al., 2015]. Remote sensing is the only means to collect repeated, consistent information of spatiotemporally variable ecosystem features across large scales. Remotely sensed variables such as vegetation indices (VIs), fraction of absorbed photosynthetically active radiation (FAPAR), and leaf area index (LAI) from multispectral sensors have been assimilated in simple light-use efficiency (LUE) and dynamic ecosystem models for monitoring and mapping GPP [Keenan et al., 2012; Running et al., 2004; Verma et al., 2015]. These variables provide reliable information of vegetation greenness and leaf area but are not sensitive to ecophysiological processes [Glenn et al., 2008] such as stomatal regulation that exert a key control on photosynthetic processes [Hilker et al., 2009].

Recently, it has become possible to sense solar-induced chlorophyll fluorescence (SIF) from space using the principle of the infilling of Fraunhofer line depth [Plascyk and Gabriel, 1975]. Studies have shown that SIF from the Greenhouse Gases Observing Satellite (GOSAT) [Frankenberg et al., 2012] and Global Ozone Monitoring Mission Experiment-2 (GOME-2) [Joiner et al., 2014] correlate well with GPP estimated by the data-driven algorithms such as MPI-BGC [Jung et al., 2011] and light-use efficiency type models such as MOD17A2

[*Running et al.*, 2004]. Because it provides a functional link with dynamic changes in photosynthetic carbon assimilation, SIF has also been integrated in land surface models such as the Soil Canopy Observation of Photosynthesis Energy Balance (SCOPE) [*Tol et al.*, 2014] and the Community Land Model (CLM) [*Lee et al.*, 2015]. Combining SIF observations from GOME-2 with the SCOPE model, recent studies have attempted to improve monthly estimates of GPP in croplands [*Guan et al.*, 2015; *Zhang et al.*, 2014].

These studies have highlighted the potential of SIF for modeling the global and mean patterns of GPP. However, the high-quality eddy covariance tower-based measurements of GPP and other relevant environmental variables are not available at the coarse spatial scales (40 by 80 km or more) comparable with the resolution of SIF retrieved from GOSAT or GOME-2. Therefore, it has not been feasible to evaluate remotely sensed SIF and empirically examine the effect of environmental conditions and physiological responses on the dynamics of the relationship between SIF and GPP. Coarse spatial resolutions of SIF also pose challenge in model validation and inversion over heterogeneous land surface, since spatially averaged high-quality measurements of input variables at a comparable resolution are not readily available for model simulations.

A process-level understanding of the dynamics between SIF and GPP at ecosystem scale is essential because the relationship between chlorophyll fluorescence and photosynthesis depends on a number of factors [*Baker*, 2008]. Less than 3 to 4% of the total photosynthetically active radiation absorbed by chlorophyll molecules fluoresces back in 680 to 800 nm range [*Krause and Weis*, 1991]. Pulse-induced chlorophyll fluorescence has been used to understand plant photosynthesis for decades in laboratory, field, and plot-level studies [*Baker and Hardwick*, 1973; *Maxwell and Johnson*, 2000]. Physiologically relevant quantitative metrics have been developed that provide a clear and precise connection between the multiple measurements and the rates of photosynthesis, fluorescence, and nonphotochemical quenching under different light conditions [*Baker*, 2008]. Remotely sensed measurement of steady state SIF, however, provides a single measurement. The information content in SIF under different environmental conditions and across different ecosystems is not precisely known, and the strength of the relationship between SIF and GPP can vary across ecosystems. As pointed out by *Porcar-Castell et al.* [2014] the spatiotemporal resolution and methodological context of the studies that use remotely sensed SIF is dramatically different from the studies that used pulse-induced chlorophyll fluorescence to investigate and model photosynthesis. Despite an exponential rise in the number of studies involving remotely sensed SIF, very little is known about the canopy level response of SIF and its relationship with GPP in varying environmental conditions in any ecosystem, let alone C4 grasslands.

Photosynthesis is a finely regulated process where plants seek to assimilate maximum energy in optimum conditions and minimize short- and long-term photochemical damage in adverse conditions such as high light or temperature [*Renger*, 2007]. Conceptualizing photosystem reaction centers in terms of open and close, *Butler* [1978] proposed a model of the partition of absorbed photosynthetically active radiation (PAR). In this model, solar photons absorbed by chlorophyll molecules have one of the three mutually exclusive fates: (i) photochemical quenching, where the excitation energy is fixed in high-energy compounds; (ii) fluorescence, where the energy is radiated back at longer wavelengths (680–800 nm); and (iii) nonradiative dissipation (NPQ), where the absorbed energy is dissipated as heat (Figure 1). In favorable conditions, bulk of the absorbed energy flows along photochemical pathways. However, suboptimal environmental and biotic conditions reduce the capacity of the plants to assimilate absorbed PAR via photochemistry. In such situations, NPQ generally increases and influences the relationship between fluorescence and photosynthesis [*Müller et al.*, 2001]. The fraction of absorbed energy that flows along each of the three pathways is thus sensitive to the dynamics of physiological stress and photoprotective mechanisms induced by environmental factors [*Flexas and Medrano*, 2002]. To integrate SIF in modeling and monitoring of GPP, we need an understanding of how SIF and GPP correlate with each other under different environmental conditions and how this relationship is mediated by NPQ

Launched in 2014, the Orbiting Carbon Observatory-2 (OCO-2) [*Crisp et al.*, 2004] has enabled fine-scale (1.3 by 2.5 km in nadir mode) and spatially dense (100-fold more than GOSAT) retrievals of SIF since September 2014 [*Frankenberg et al.*, 2014]. Due to its relatively fine spatial resolution and its ability to take multiple measurements in a small area, OCO-2 provides the first satellite-based SIF retrievals that can be directly compared with the meteorological and eddy covariance flux measurements recorded at flux towers. OCO-2 also flies in the A-train constellation with the Moderate Resolution Imaging Spectroradiometer

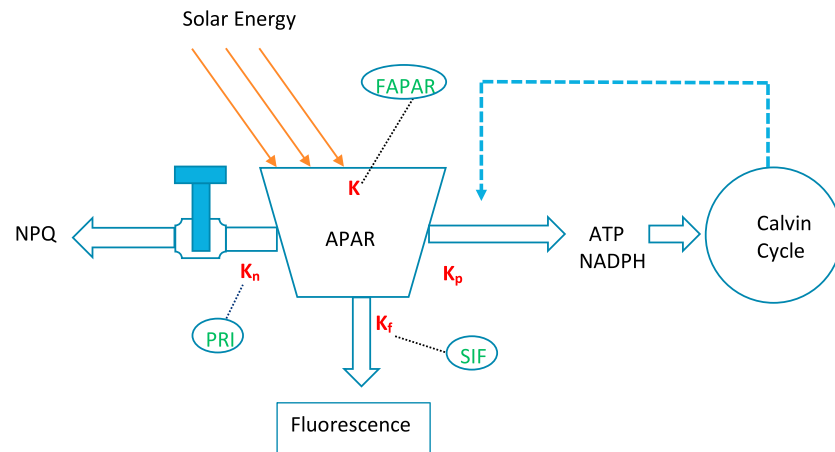


Figure 1. Conceptual diagram showing partition of absorbed photosynthetically active radiation (APAR) in three main, mutually exclusive pathways: photochemistry, fluorescence, and nonradiative decay known as nonphotochemical quenching (NPQ). K is the rate of energy absorption (APAR). K_p , K_n , and K_f are the rates at which APAR flows along photochemical, fluorescence, and NPQ pathways, respectively, such that the sum of the three rates equals K [Govindjee *et al.*, 1987]. Any imbalance in the rate at which ATP and NADPH are produced in the light reaction and later utilized in the Calvin cycle feeds back and causes a reduction in K_p , which in turn affects K_n and K_f . The blue knob along the NPQ path underlines the fact that K_n is a physiologically regulated flux, and plants can increase or decrease it depending on the amount of excess energy. Remotely sensed fraction of absorbed photosynthetically active radiation (FAPAR), solar-induced fluorescence (SIF), and photochemical reflectance index (PRI) give us information of K , K_f , and K_n , respectively.

(MODIS) on board the Aqua satellite and the instruments on the two satellites take measurements within 15 min from each other in nearly identical conditions with comparable spatial resolution. This facilitates integration of complementary measurements from MODIS and OCO-2 on different aspects of vegetation functions. A key physiological mechanism driving NPQ is the deepoxidation of the xanthophyll cycle pigments [Demmig-Adams and Adams, 1996], which causes a decrease in reflectance around 531 nm. This change in reflectance can be detected via the photochemical reflectance index (PRI) derived from MODIS Aqua data [Gamon *et al.*, 1992; Garbulska *et al.*, 2011]. Although confounded by many factors such as viewing geometry and chlorophyll-carotenoid ratio, PRI can provide information of variability in NPQ. Together, OCO-2 and MODIS Aqua thus have the potential to deliver simultaneous, coincident measurements of SIF and PRI and help us understand dynamic changes in the relationship between SIF and GPP.

In this study, we combine OCO-2 SIF with in situ measurements and data from MODIS to examine the effect of environmental conditions and ecophysiological responses on the relationship between SIF and GPP at a well-characterized natural grassland site. The site is located in the extensive Mitchell Grasslands of the Northern Territory, a large homogeneous area dominated by a single C₄ grass species, in Australia. Previous studies [Frankenberg *et al.*, 2012; Guanter *et al.*, 2012] investigated the relationship of SIF with GPP at a monthly time scale, which was appropriate for establishing a statistical relationship between the two. However, photosynthesis and SIF respond to environmental changes at almost an instantaneous time scale. Therefore, mean monthly (or biweekly) SIF and GPP provide little or no information about how environmental conditions and NPQ mediate the dynamic relationship between SIF and GPP. Because our primary motivation is to understand this dynamic relationship at canopy and ecosystem level, we focus on the instantaneous time scales at the satellite overpass time when the biological basis for a dynamic relationship amongst SIF, APAR, and GPP is strong (Figure 1), and the potential for understanding how environmental conditions and physiological regulations affect their mutual relationship is high. The actual quantum of energy that flows along photochemical and fluorescence pathways depends on the total absorbed energy and the rate of flow along each (Figure 1). Based on field- and leaf-level studies, we hypothesize that for the environmental conditions (tropical savannas) and vegetation (C₄ grass) found at the selected site, SIF and GPP would correlate strongly in low to medium light, temperature, and vapor pressure deficit (VPD). However, the relationship may become nonlinear [Porcar-Castell *et al.*, 2014] or even change the direction when light saturation occurs because of high incoming light, stomatal closure, or reduction in enzymatic activity. In

such conditions, physiologically regulated xanthophyll cycle enables plants to dissipate extra energy safely and protect photosystems from oxidative stress. As this nonphotochemical dissipation of energy becomes significant, it reduces the efficiency of photochemistry and fluorescence affecting the relationship between SIF and GPP.

In addition to investigating the empirical relationship between SIF and GPP, we also examine the capacity of the SCOPE model to predict OCO-2 SIF at the time of satellite overpass and assess how well OCO-2 SIF constrains the estimates of the maximum carboxylation capacity (V_{cmax}) of RuBisCO, an important parameter in the model. SCOPE is the first model to predict ecosystem level SIF and relate it to GPP. Because of these innovations, it has played an important role in utilizing SIF from GOME to improve estimates of V_{cmax} and GPP [Zhang *et al.*, 2014]. However, recent studies have pointed out that the sensitivity of SIF to V_{cmax} in the SCOPE model is weak [Koffi *et al.*, 2015; Verrelst *et al.*, 2015, 2016]. It had not been possible to rigorously examine the predictive power of the SCOPE model because the forcing, canopy reflectance, and GPP data are not available at a spatial resolution comparable with GOSAT and GOME-2. Here we combine comparable data from OCO-2 SIF, MODIS, and an eddy covariance tower with a canopy radiative transfer model, PROSAIL [Jacquemoud *et al.*, 2009], and the SCOPE model to examine how well SCOPE predicts SIF and to what extent can we use OCO-2 SIF to constrain V_{cmax} and improve GPP estimates. We focus on the instantaneous time scale at the satellite overpass time so that we can examine the accuracy of predicted SIF and assess the reliability of the biological mechanisms, formalized in the model, that relate SIF to GPP.

2. Materials and Methods

To realize the objectives identified above in section 1, we combined observations from OCO-2 and MODIS, measurements from an eddy covariance tower, and simulations from the PROSAIL and SCOPE models. In this section, we first describe site characteristics and tower measurements, next, we cover OCO-2 and MODIS data used in the study, followed by the details of the simulation of the two models, and finally, we describe the statistical analyses carried out to accomplish the objectives.

2.1. Field Site and Measurements

We employed eddy covariance and meteorological measurements from Sturt Plains, an open savanna grassland site in the Australian regional flux network (OzFlux). A comprehensive overview of the OzFlux network is given in Beringer *et al.* [2016]. The Sturt Plains site was established in 2008 as part of a campaign to understand the spatial patterns of carbon and water fluxes across the landscape. The campaign utilized a transect (North Australian tropical transect (NATT)) that follows a strong continental rainfall gradient [Beringer *et al.*, 2011a, 2011b]. The details of the flux sites along the NATT are provided in Hutley *et al.* [2011]. Here we include a summary of the salient features of the Sturt Plains site. The site is located at 17.1507°S and 133.3504°E at an elevation of 225 m. Based on the 0.1° resolution gridded data from the Bureau of Meteorology between 1961 and 1990, the site had a mean annual temperature of approximately 26°C and precipitation of 750 mm [see Beringer *et al.*, 2016, Figure 2]. Tower data collected between 2008 and 2014 showed that nearly 90% of the rain falls in the growing season between December and April. The site is dominated by Mitchell grass, a perennial, tussock grass that grows between November and April and occupies an area of 93,000 km² across the Northern Territory and Queensland [Fox *et al.*, 2001]. It not only plays an important role in the regional biogeochemistry and carbon cycle, but also sustains the local cattle-based livestock systems.

We employed air temperature, incoming solar radiation, VPD, precipitation, and GPP data, collected at 30 min resolution, from the tower records. We also utilized soil moisture in the top 3 cm layer, which was modeled from measured precipitation. We assumed that the photosynthetically active radiation (PAR) was 47% of total incoming solar radiation [Kannah *et al.*, 2012]. Eddy covariance systems measure net ecosystem exchange (NEE), which is the net sum of GPP and respiration. To derive GPP, respiration was first modeled by calibrating an empirical temperature response function to nighttime data when there is no photosynthesis and NEE is equal to respiration [Beringer *et al.*, 2016]. It was assumed that the relationship calibrated using nighttime data remains the same during the daytime, and GPP was estimated by subtracting modeled daytime respiration from measured NEE.

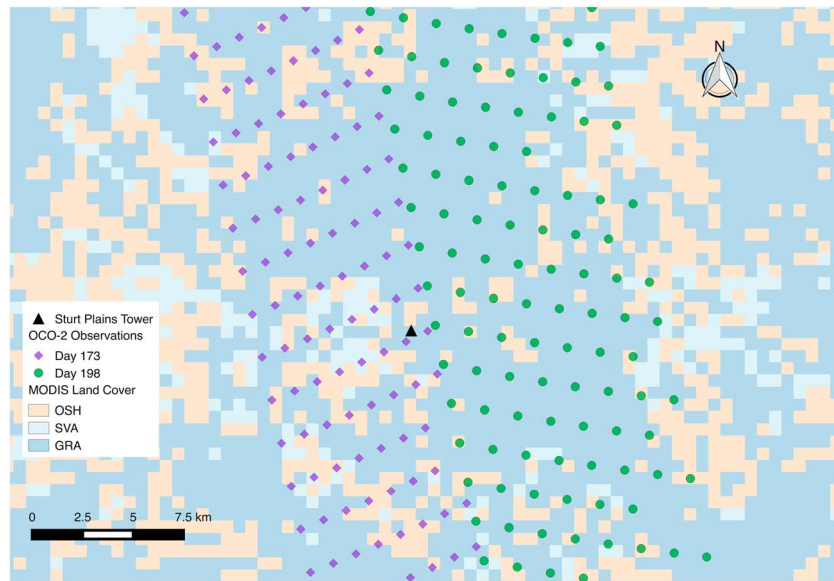


Figure 2. OCO-2 observations near the Sturt Plains site for day of year 173 and 198 in 2015, overlaid on the MODIS land cover product (MCD12Q1). Observations on day of year 173 were recorded in the nadir mode, and on day 198 in the glint mode with a sensor zenith angle of 44.5° . In the legend above, OSH, SVA, and GRA are open shrublands, savannas, and grasslands, respectively.

2.2. SIF From OCO-2

OCO-2 flies in a polar, Sun-synchronous orbit leading the A-train constellation with an equatorial crossing time of 1:35 P.M. [Hammerling *et al.*, 2012]. It carries three spectrometers to measure reflected radiances centered at 760 (O₂ A-Band, from 757 to 775 nm), 1610 (weak CO₂-Band), and 2060 nm (strong CO₂-Band) at a very high spectral resolution with a resolving power ($\lambda/\Delta\lambda$) of 17,000 in the O₂ A-Band [Frankenberg *et al.*, 2015]. The spectrometers collect reflected light from sampled locations in eight independent along-slit focal plane readouts (Figure 2). Measurements are collected in the nadir and glint mode alternatively with a repeat frequency of approximately 16 days. The spatial resolution of each measurement is 1.3 by 2.5 km in the nadir mode with a total swath width of 10.6 km.

SIF is retrieved following the idea of the infilling of Fraunhofer line at 757 and 771 nm wavelength from the observations recorded in the O₂ A-Band [Frankenberg *et al.*, 2014]. Emissions due to inelastic Raman scattering in the atmosphere can also fill in Fraunhofer lines. However, this effect is relatively small compared to the effect of chlorophyll fluorescence on Fraunhofer line infilling [Vasilkov *et al.*, 2013]. Although, the SIF signal is small, it is possible to detect it even in moderately cloudy conditions up to a cloud optical thickness of 5 [Frankenberg *et al.*, 2012].

OCO-2 started collecting data on 6 September 2014. Although, OCO-2 collects spatially dense sample along its line of light, because of a short swath width (10.3 km), OCO-2's global coverage of terrestrial area is extremely sparse (see Figure S1 in the supporting information to get an idea of the area covered by a typical day's successful retrievals of SIF). Because of this sparse coverage, temporally dense (more than 10 well-spaced observations over a season) SIF data were not available for most flux tower sites in the OzFlux network. Sturt Plains was the only site where we had 14 temporally well-spaced retrievals of SIF near the flux tower site (Table 1) and was located in a spatially homogeneous area (Figure 2) dominated by a single C4 species, Mitchell grass (*Astrebla* sp.). We downloaded SIF "lite" files in NetCDF format from <https://co2.jpl.nasa.gov/> containing data between 6 September 2014 and 11 August 2015, a period that corresponds to a full seasonal cycle in the Southern Hemisphere, and extracted data in the vicinity of the Sturt Plains site. In addition to SIF, the NetCDF files also contain information about solar and sensor geometry and include a correction factor which is the ratio of instantaneous PAR at the time of overpass to daily PAR in clear-sky conditions. To a first order, this correction factor converts instantaneous SIF to a daily average.

Table 1. Details of the 14 SIF Observations Recorded by OCO-2 Near Sturt Plains

No.	Year	Date	Day of Year	Local Time of Overpass	Mode of Observation	Solar Zenith Angle at Overpass (deg)
1	2014	9 Oct	282	14:23	Nadir	30.9
2	2014	26 Nov	330	14:22	Nadir	28.3
3	2014	28 Dec	362	14:22	Nadir	25.3
4	2015	29 Jan	29	14:22	Nadir	22.3
5	2015	7 Feb	38	14:17	Glint	20.7
6	2015	2 Mar	61	14:23	Nadir	25.3
7	2015	11 Mar	70	14:17	Glint	26.0
8	2015	3 Apr	93	14:23	Nadir	34.3
9	2015	12 Apr	102	14:17	Glint	35.7
10	2015	21 May	141	14:22	Nadir	46.2
11	2015	22 Jun	173	14:23	Nadir	47.9
12	2015	1 Jul	182	14:16	Glint	46.5
13	2015	8 Jul	189	14:23	Nadir	46.7
14	2015	17 Jul	198	14:16	Glint	44.6

The SIF data were available within a circle of 25 km radius from the tower 14 times between September 2014 and August 2015 (Table 1 and Figure 2). Although the repeat frequency of OCO-2 is 16 days, because of the issues such as the thermal conditions of the instruments, the actual average temporal frequency of SIF retrievals near Sturt Plains was about 25 days. The SIF signal at 757 nm is expected to be relatively stronger than at 771 nm. To give equal weight to both the signals, we multiplied the weaker signal with 1.4 and calculated the mean of the two retrievals. We estimated SIF at the tower site by taking the mean of all the pixels that had the similar land cover as the tower site within the circle.

2.3. MODIS Data and PRI

We downloaded nadir bidirectional reflectance distribution function (BRDF)-adjusted reflectance (NBAR; MCD43A4) [Schaaf *et al.*, 2002] data from MODIS from the Oak Ridge National Laboratory Distributed Active Archive Center (ORNL DAAC; <https://daac.ornl.gov/>). We employed these data to constrain PROSAIL simulations (described later in section 2.4). We also obtained data for band 11 (526–536 nm), 12 (546–556 nm), and 13 (662–672 nm) recorded by MODIS Aqua from the National Aeronautics and Space Administration’s (NASA) Level 1 and Atmosphere Archive and Distribution System (LAADS Web; <https://ladsweb.nascom.nasa.gov/>) for the days that coincided with the availability of SIF data from OCO-2 (Table 1). We utilized the bands 11, 12, and 13 to estimate PRI [Drolet *et al.*, 2008; Garbulsky *et al.*, 2011]. As described earlier, MODIS on board the Aqua platform flies with OCO-2 in the A-train constellation and records measurements about 15 min after OCO-2 in nearly identical conditions. PRI calculated with bands 12 and 13 showed identical seasonal variability, and thus, for all the analyses in this study we employed band 12 and defined PRI as in equation (1) below.

$$PRI = \frac{\rho_{526-536} - \rho_{546-556}}{\rho_{526-536} + \rho_{546-556}} \quad (1)$$

where $\rho_{546-556}$ and $\rho_{526-536}$ are at-sensor reflectance from MODIS bands 12 and 11, respectively. Following Drolet *et al.* [2008] and Goerner *et al.* [2011], we assumed that the atmospheric effects were small and similar (but see section 4 about the effect of atmospheric correction on PRI) across all the measurements and calculated scaled PRI (sPRI) as

$$sPRI = \frac{1 + PRI}{2} \quad (2)$$

Over seasonal time scales sPRI is sensitive to canopy structure and pigment pools [Hall *et al.*, 2008; Hilker *et al.*, 2009]. For the morphologically simple grassland vegetation at Sturt Plains, seasonal variability in canopy structure and pigment pools is captured by EVI at first order. Thus, to minimize the effects of seasonal variability in canopy structure and pigment pools, we normalized sPRI by EVI and assumed that the remaining variability in sPRI was due to the dynamics of the xanthophyll cycle. This normalization procedure is designed to correct for the constitutive (pigments and structure changing over seasonal time scales) effects that have

Table 2. Values of the Key Parameters and Inputs Used in the Simulation of the PROSAIL (PROSPECT + SAIL) Model^a

Parameter	Unit	Minimum Value	Maximum Value
<i>PROSPECT</i>			
Leaf chlorophyll content	$\mu\text{g cm}^{-2}$	5	80
Leaf structural parameter	unitless	1.4	1.6
Dry matter content	g cm^{-2}	0.0025	0.01
Equivalent water thickness	cm	0.01	0.02
<i>SAIL</i>			
Leaf area index	unitless	0.1	2
Leaf angle distribution	unitless	erectophile distribution ($\text{LIDF}_a = -1$; $\text{LIDF}_b = 0$)	
Observer zenith angle	deg	nadir	nadir
Solar zenith angle	deg	at the time of satellite overpass	
Hot spot parameter	unitless	0.01	0.01

^aAll parameters with different minimum and maximum values were assumed to have a uniform distribution between the upper and lower bounds.

been shown to influence the interpretation of the facultative component that effects NPQ via xanthophyll deepoxidation [Filella et al., 2009; Garrity et al., 2011; Sims and Gamon, 2002]. Correcting for these confounding effects from satellite data with a single overpass in a day is challenging. As such, we suggest that the normalized sPRI is more representative of the facultative component of the PRI signal [Gamon and Berry, 2012; Magney et al., 2016; Zarco-Tejada et al., 2013]. In a recent development, Gamon et al. [2016] have suggested to interpret PRI-type ratio as an indicator of change in pigment ratios in the context of evergreen needleleaf forests. How far this interpretation applies to savanna grasslands remains to be investigated. However, since these ratios actually change at a pretty rapid time scale, we can assume that the bulk carotenoids that are being replaced are from bulk xanthophylls and more bulk xanthophylls in the system suggests the greater potential for deepoxidation.

2.4. PROSAIL and SCOPE Simulations

To evaluate the predictive power SCOPE and to assess the robustness of the mechanisms formalized in it, we compared SIF predicted by SCOPE with OCO-2 SIF and also assessed how well does OCO-2 SIF constrain the estimates of V_{cmax} . Over the course of a season instantaneous relationship between SIF and GPP at the satellite overpass time is affected both by changes in canopy structure as well as physiology. To minimize the confounding effects of structure, we simulated the PROSAIL and SCOPE models in a sequential, two-step process. We first utilized MODIS reflectance with the PROSAIL model to retrieve seasonal variations in canopy structure (e.g., LAI) and leaf Chlorophyll (Cab). In the past two decades, PROSAIL has been used in several studies [Jacquemoud et al., 2009, and references therein] to simulate the expected top of canopy reflectance observed from remote sensing. These studies have shown that the inversion of PROSAIL with remotely sensed reflectance data provides robust estimates of changes in canopy structure. Note that although we had only 14 measurements of SIF (Table 1), we had 46 (every 8 days) estimates of surface reflectance and vegetation indices to constrain and invert seasonal changes in canopy structure.

In the next step, we ingested leaf and canopy variables retrieved from the PROSAIL model as prescribed inputs in the simulation of the SCOPE model to understand how well the feedback mechanisms amongst fluorescence, photosynthesis, and NPQ enables SIF to constrain V_{cmax} .

PROSAIL is a radiative transfer model that couples a leaf-level model, PROSPECT [Ferret et al., 2008; Jacquemoud and Baret, 1990], with a canopy radiative transfer model, SAIL [Verhoef, 1984], and has been widely used in several studies over the last 20 years [Zhang et al., 2005; Jacquemoud et al., 2009]. PROSAIL formalizes plant canopies as horizontally homogeneous randomly distributed media that are bounded at bottom by a reflecting soil surface. This one-dimensional random media representation is a reasonable approximation for short, morphologically simple, and homogeneous vegetation found at the Sturt Plains site. At low LAI, PROSAIL simulations are sensitive to soil reflectance. To prescribe realistic soil reflectance, we located "pure-soil" pixels in the MODIS data in the vicinity of the tower and modified the dry-soil reflectance spectrum used in PROSAIL based on these pixels. We assumed a linear decay in reflectance due to soil moisture and applied modeled soil moisture at 3 cm to modify the reflectance of soil at each time step.

Table 3. Values of Key Parameters Employed in the Simulation of the SCOPE (Version 1.61) Model

Parameter	Unit	Value
V_{cmax}	$\mu\text{mol m}^{-2} \text{s}^{-1}$	10, 30, 60, 90, 120, 150, 180
Ball-Berry stomatal conductance parameter	unitless	8
Photochemical pathway	unitless	1 (C_4)
Extinction coefficient for V_{cmax}	unitless	0.6396
Mean annual temperature	$^{\circ}\text{C}$	26
Fraction of photons partitioned to PSII	unitless	0.4
Fraction of functional reaction centers	unitless	1
Stress factor	unitless	1
Fluorescence quantum yield efficiency at photosystem level	unitless	0.01
Fluorescence model		0 (Fit to Felxas' data)
Vegetation height	meter	2
Leaf width	meter	0.1
Measurement height of meteorological data	meter	5
CO_2 concentration	ppm	395
O_2 concentration	per mil	209
Roughness length for momentum of the canopy	meter	0.246
Displacement height	meter	1.34
Leaf drag coefficient	unitless	0.3
Leaf boundary resistance	s m^{-1}	10
Solar zenith angle	deg	at the time of OCO-2 overpass
Sensor zenith angle	deg	at the time of OCO-2 overpass

Following previous studies [Darvishzadeh *et al.*, 2008; Knyazikhin *et al.*, 1998] and our knowledge of the vegetation at the tower site, we assumed an erectophile leaf angle distribution. We sampled the entire feasible parameter space (Table 2) at fine resolution and simulated top of canopy reflectance for the middle of each 8 day period coinciding with the availability of MODIS NBAR-corrected reflectance data. We extracted MODIS reflectance in a three-by-three window centered at the Sturt Plains site. We assumed that standard deviation across space was a robust measure of the variability at each time step at Sturt Plains. Finally, we selected the parameter vectors that minimized discrepancy between the simulated and MODIS vegetation indices (Figure S2 in the supporting information) within the margins of error.

In the next step, we combined PROSAIL derived parameters such as leaf chlorophyll concentration and LAI with tower data from the Sturt Plains site and simulated the SCOPE model (version 1.61) in forward mode at the time of OCO-2 overpass. SCOPE is a land surface model that simulates fluorescence, photosynthesis, net radiation, and latent and sensible heat flux [Tol *et al.*, 2014, 2009]. Absorbed photons in SCOPE can take one of the three pathways—photochemistry, fluorescence, or nonradiative dissipation (NPQ)—with different probabilities such that the sum of the three probabilities is always 1, coupling photochemistry with fluorescence. We used instantaneous incoming solar radiation, temperature, pressure, wind speed, and humidity from tower measurements. We utilized site information and tower data to realistically assign parameters such as zero plane displacement, roughness height, and mean annual temperature (Table 3) and simulated SCOPE at the OCO-2 overpass time (Table 1) over the season at Sturt Plains. We assigned seven different values of V_{cmax} , 10, 30, 60, 90, 120, 150, and $180 \mu\text{mol m}^{-2} \text{s}^{-1}$. Tower data showed that peak daily GPP was between 4 and $6 \text{ gC m}^{-2} \text{ d}^{-1}$ between 2008 and 2014. Given this rate of peak productivity, a V_{cmax} range from 10 to $180 \mu\text{mol m}^{-2} \text{s}^{-1}$ (Table 3) covered the possible range for the C_4 grasses present at the Sturt Plains site. Note that our primary objective was to examine if OCO-2 SIF can be used to constrain the estimates of V_{cmax} and thereby test if the assumptions formalized in SCOPE were valid at Sturt Plains or not.

2.5. Analyses

To understand how the dynamics of photoprotective mechanisms induced by high light and environmental stress affect the relationship between SIF and GPP, we defined an environmental index by combining APAR, air temperature, and VPD at the time of OCO-2 overpass. First, we linearly transformed each of the three variables (APAR, air temperature, and VPD) between 0 and 1 with respect to the minimum and maximum observed over the season [Mu *et al.*, 2011; Running *et al.*, 2004]. For each of the three variables we chose a minimum that was a fraction (5%) less than the observed minimum. This allowed us to have a nonzero,

positive scaled value at the observed minimum. For example, for every day of the overpass of OCO-2, scaled APAR was calculated as follows:

$$S_{\text{APAR}}^d = \frac{\text{APAR}^d - \text{APAR}_{\text{min}}}{\text{APAR}_{\text{max}} - \text{APAR}_{\text{min}}} \quad (3)$$

where APAR is the 30 min actual APAR measurement that overlapped with the OCO-2 overpass time on day “d,” APAR_{min} is the minimum 30 min APAR, and APAR_{max} is the maximum of 30 min APAR recorded at the time of OCO-2 overpasses over the season. We then created a composite quantity, S , by adding the three scaled scalars to estimate the combined effect of the environmental conditions and linearly scaled it between 0 and 1 to create an Environmental Condition Index (ECI) [Anand, 1994; Anand and Sen, 2000]. Very high values of ECI corresponded to conditions when APAR, temperature, and VPD were high.

Note that our motivation is to use ECI for identifying conditions where canopies are likely to be in stress. We do not propose that ECI tracks environmental stress linearly. Instead, we suggest that on average canopies are likely to have excess PAR when ECI is high (>0.8) relative to when it is low. Also note that both EVI and incident PAR caused APAR to change over the course of the season. As solar zenith angle increases, the intensity of incoming PAR decreases because the same amount of radiation falls on a larger area. In addition, increase in zenith angle also increases atmospheric attenuation because of an increase in path length, further decreasing the incoming PAR. Over the course of the season, however, EVI also changed significantly and played a larger role in moving APAR up and down.

We compared SIF with GPP at the time of satellite overpass and also analyzed the relationship between LUE and SIF yield, and between normalized sPRI and SIF yield at the satellite overpass time. We calculated APAR as PAR multiplied by EVI [Mahadevan et al., 2008; Xiao et al., 2004], LUE as GPP normalized by APAR, and SIF yield as SIF normalized by APAR. As described earlier, GPP and incoming PAR were obtained from tower data for the 30 min period that overlapped with satellite overpass time (Table 2). To understand the effect of environmental conditions on these relationships, we utilized ECI from equation (3) above. We also examined if SIF yield and sPRI together could give better information of LUE.

In the second part of the study, we compared SCOPE-predicted SIF at the time of satellite overpass with OCO-2 SIF and also analyzed the relationship between SCOPE-predicted instantaneous GPP and corresponding 30 min GPP derived from tower data for the six different values of V_{cmax} : 30, 60, 90, 120, 150, and $180 \mu\text{mol m}^{-2} \text{s}^{-1}$.

3. Results

3.1. Environmental Conditions at the Time of Satellite Observations

Instantaneous air temperature, VPD, and APAR varied between 39 and 20°C (mean = 32°C), 6.4 and 1.6 kPa (mean = 3.63 kPa), and 125 and 38 W m^{-2} (mean = 70 W m^{-2}), respectively, at the time of satellite overpass. Over the season, normalized-APAR (S_{APAR}) showed a relatively smooth variation (Figure 3b). However, vegetation experienced fluctuating air temperature and VPD at the time of overpass (Figure 3a). Normalized air temperature and VPD correlated with each other strongly ($r = 0.79$; Figure 3a).

ECI summarized the information in the three environmental variables very well (Figures 3a and 3b) and afforded a simple and objective metric to map the range of environmental conditions experienced by the vegetation and photosynthetic apparatus. On four occasions ECI was more than 0.8. One of the four highest values occurred in early October when the growing season had not yet begun and the high value was driven primarily by a very high temperature and VPD. The remaining three high values occurred during the peak growing season between January and March and marked the instances when the vegetation at Sturt Plains was exposed to high light, temperature, and VPD. The three ECI values, thus, likely identify instances when the photoprotective mechanisms are likely to be more active than the other occasions.

3.2. Relationship Amongst SIF, GPP, and PRI

Instantaneous SIF varied from 0 to $1 \text{ W m}^{-2} \mu\text{m}^{-1} \text{ sr}^{-1}$ and correlated strongly with 30 min GPP ($r = 0.91$, p value < 0.0001 ; Figure 4a) at the satellite overpass time over the season under a range of environmental conditions. Instantaneous SIF yield also showed a strong linear relationship with instantaneous LUE ($r = 0.89$, p value < 0.0001 ; Figure 4b). The highest values of SIF and GPP, and SIF yield, and GPP occurred

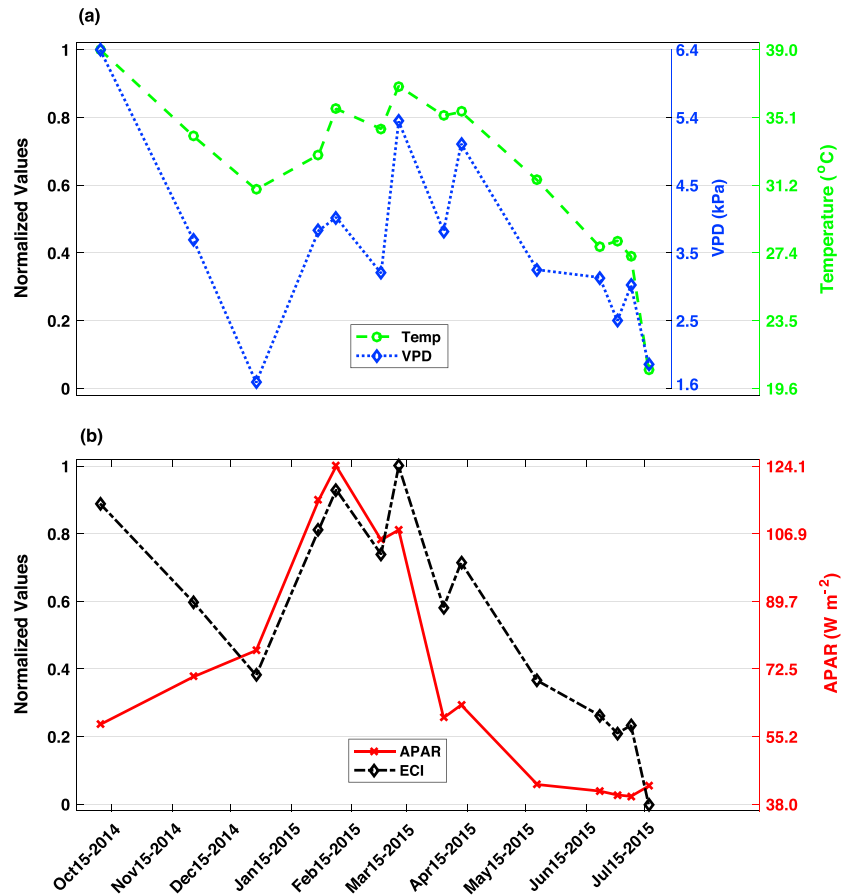


Figure 3. Seasonal trajectories of normalized (scaled between 0 and 1) (a) air temperature (T_{air}) and VPD, and (b) APAR and ECI at the time of OCO-2 and MODIS overpass at Sturt Plains. See section 2.5 for how normalized values were calculated.

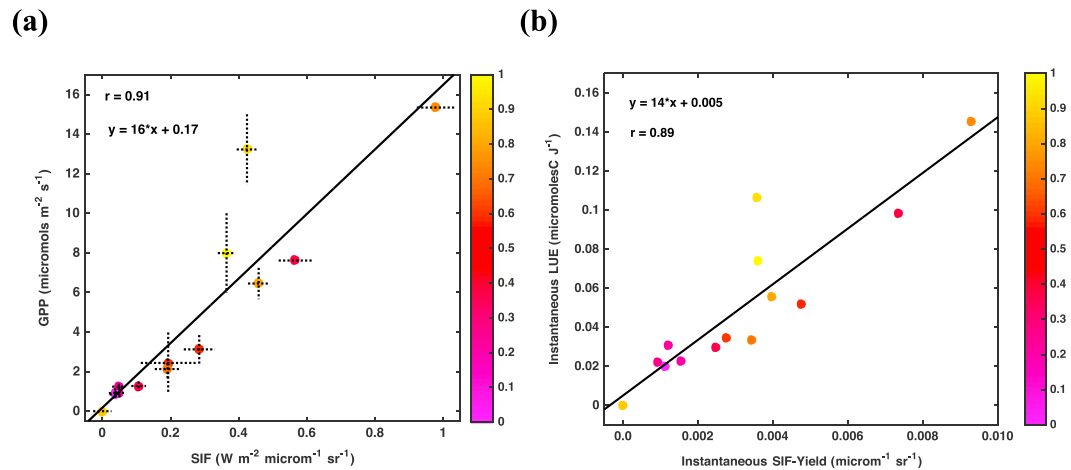


Figure 4. Relationship between solar-induced fluorescence (SIF) from the (a) Orbiting Carbon Observatory-2 (OCO-2) and 30 min GPP from eddy covariance tower, and (b) SIF yield (SIF/APAR) and light-use efficiency over a season at the satellite overpass time at Sturt Plains, an OzFlux grassland site in northern Australia. Each point is colored with ECI (see section 2.5 and Figures 3a and 3b), a composite index derived from APAR, temperature, and VPD that varies between 0 and 1 and captures the environmental conditions experienced by the vegetation at the time of satellite overpass. High values of ECI are likely to indicate conditions of excel light and ecophysiological stress.

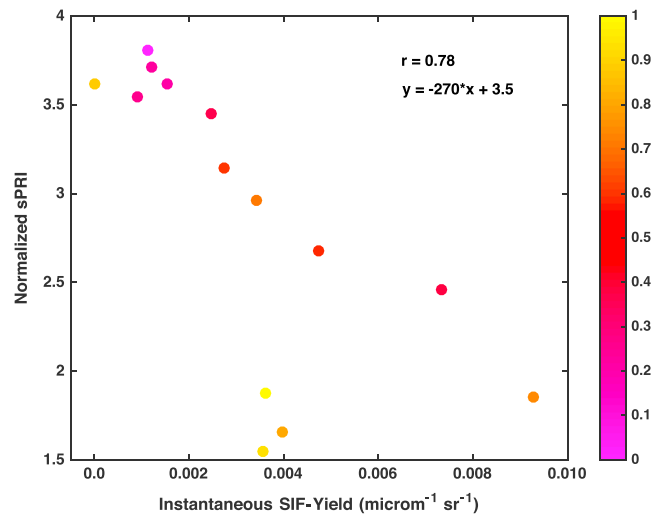


Figure 5. Relationship of instantaneous SIF yield with normalized sPRI at Sturt Plains, an OzFlux grassland site in northern Australia. Each point is colored with ECI (Environmental Conditions Index, see section 2.5), an index that varies between 0 and 1 and captures the environmental conditions experienced by the vegetation at the time of satellite overpass. High values of ECI are likely to indicate conditions of ecophysiological stress when NPQ is likely to be more.

when APAR and temperature were approximately 75% of the maximum value ($S_{\text{APAR}} = 0.76$ and $S_T = 0.75$) and VPD was low ($S_{\text{VPD}} = 0.34$; Figures 3 and 4).

Instantaneous SIF yield also correlated well with normalized sPRI ($r = 0.78$, p value < 0.0001 ; Figure 5). However, the linear relationship broke down for ECI values greater than 0.8. (The three points that lie below the fitted line in Figure 5 corresponded to ECI higher than 0.8.) Using SIF yield and normalized PRI together as predictors in a multiple linear regression framework improved the correlation between the measured and predicted LUE marginally ($r = 0.94$; p value < 0.0001).

Most previous studies have used monthly mean SIF from GOSAT or GOME-2 to estimate integrated monthly GPP [Guanter *et al.*, 2012]. Although our focus is on the instantaneous time scales at satellite overpass time, to assess how results from OCO-2 matched with previous studies, we compared monthly mean SIF with monthly integrated GPP at Sturt Plains. Relative to the instantaneous scale, we noticed a weaker relationship ($r = 0.68$, results not shown) between the monthly mean SIF and integrated monthly GPP.

3.3. Relationship Between SCOPE and OCO-2 SIF

LAI and leaf chlorophyll content (Cab) derived from the PROSAIL simulations showed the familiar seasonal pattern but with a noticeable midseason dip (Figure 6). The maximum LAI was close to 1, and the maximum chlorophyll content (Cab) was about $45 \mu\text{g cm}^{-2}$ (Figure 6). We applied the nearest neighbor interpolation and estimated LAI and Cab values at the days of OCO-2 overpass. These interpolated LAI and Cab values were used as input data in the simulation of the SCOPE model.

Figure 7 shows the seasonal trajectories of SIF from OCO-2 along with the SIF modeled by the SCOPE model for the V_{cmax} values of 30, 90, and $180 \mu\text{mol m}^{-2} \text{s}^{-1}$. Because the modeled SIF values did not diverge away from one another significantly for different V_{cmax} , we show the simulated SIF for only three different values. V_{cmax} had little impact on the agreement between the modeled and OCO-2 SIF (Figure 7).

Simulated SIF from the SCOPE model correlated with OCO-2 SIF over the season with a correlation coefficient of 0.84, 0.85, 0.84, 0.83, 0.82, 0.82, and 0.81 (p value < 0.001) for the V_{cmax} values of 10, 30, 60, 90, 120, 150, and $180 \mu\text{mol m}^{-2} \text{s}^{-1}$, respectively. The (RMSE) between the simulated and OCO-2 SIF was 0.24, 0.22, 0.20, 0.20, 0.20, 0.21, and 0.21 for the V_{cmax} values of 10, 30, 60, 90, 120, 150, and $180 \mu\text{mol m}^{-2} \text{s}^{-1}$, respectively.

The modeled SIF was consistently lower than the OCO-2 SIF. The peak SIF from the SCOPE model was nearly half of the peak SIF from OCO-2. SIF from the SCOPE model did not show the conspicuous steep rise in the middle of the season exhibited by the OCO-2 SIF, nor did it display the midseason dip noticeable in the remotely sensed SIF (Figure 7).

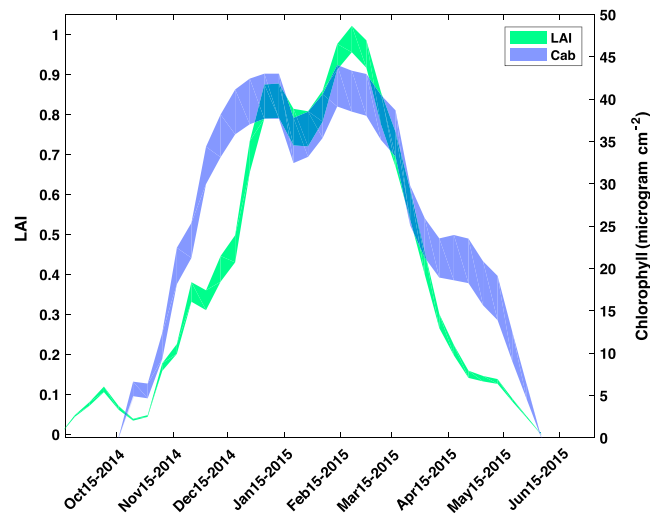


Figure 6. Seasonality of leaf area index (LAI) and chlorophyll (Cab) retrieved by inverting the PROSAIL model with MODIS reflectance.

Although V_{cmax} had little impact on the simulated SIF, it had a significant and monotonous effect on GPP (results not shown) with peak GPP values varying more than 8 times between the minimum ($10 \mu\text{mol m}^{-2} \text{s}^{-1}$) and the maximum ($180 \mu\text{mol m}^{-2} \text{s}^{-1}$) values of V_{cmax} .

4. Discussion

We observed a strong linear correlation between SIF and GPP, SIF yield and LUE, and sPRI and SIF yield at the instantaneous time scale (Figures 4a, 4b, and 5). The relationship between SIF and GPP, and SIF yield and LUE appeared significantly robust to changes in environmental conditions. Based on the leaf-level studies, we hypothesized (see section 1) that the relationship between fluorescence and photosynthesis may become nonlinear or change direction when absorbed PAR is significantly higher than what can be assimilated in photochemistry. We did not see evidences of a significant nonlinearity or a change in the direction of the relationship between SIF (SIF yield) and GPP (LUE). Although one of the points with high ECI values deviated

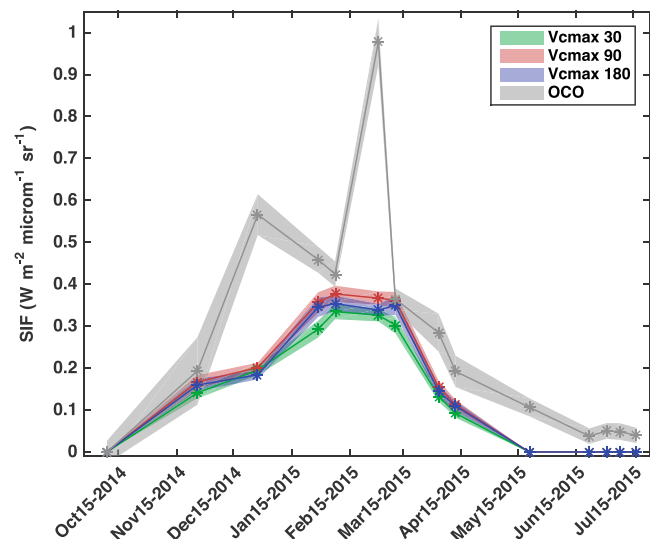


Figure 7. Seasonality of OCO-2 SIF and top of canopy fluorescence modeled by SCOPE for three different values of the maximum carboxylation capacity (V_{cmax}) of RuBisCO at Sturt Plains for the 14 days when OCO-2 SIF data were available.

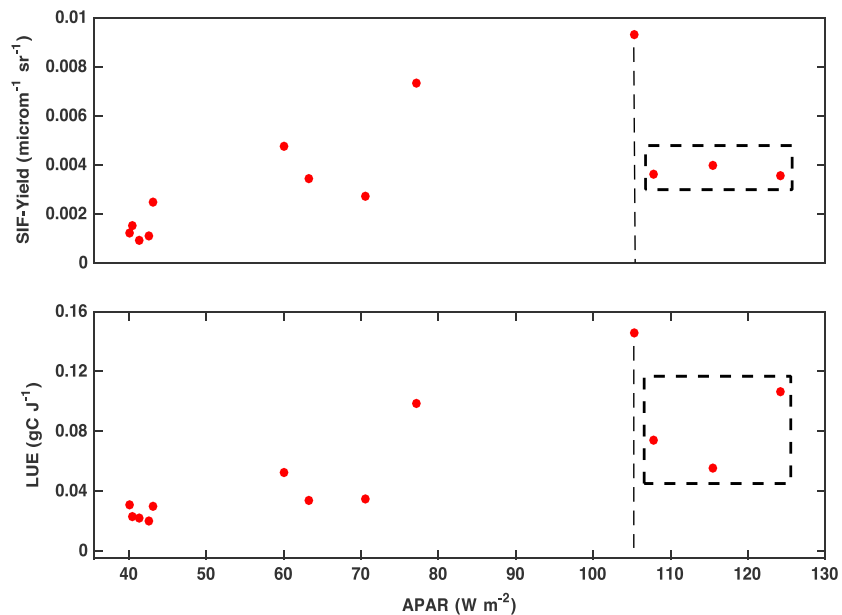


Figure 8. Variation in light-use efficiency and SIF yield as a function of absorbed PAR over the course of a season at Sturt Plains. The three points in the box correspond to the points that deviate away from the least squares line in Figure 5.

away from the linear relationship (Figures 4a and 4b), overall, the relationship remained linear under a range of APAR, air temperature, and VPD values (Figure 3). Our results thus generate greater confidence in utilizing SIF for modeling ecosystem level GPP in a range of ambient conditions.

Excess-light-induced physiological stress is known to affect fluorescence and photochemical yield. Because fluorescence, NPQ, and photochemistry are mutually exclusive and competing pathways, changes in the efficiency of one affects the efficiency of the other two pathways [Maxwell and Johnson, 2000]. Stress-induced shutdown of photochemical traps in photosystem-II causes fluorescence yield to increase as the lifetime of excited electrons increases. On the other hand, stress-induced opening up of additional NPQ channels causes fluorescence to drop [Mohammed et al., 2014]. However, both the closing down of reaction centers as well as the opening of NPQ channels result in a drop in photochemical yield. The effects of the increase in NPQ on SIF yield and LUE may or may not be proportional. When the decrease in both SIF yield and LUE is proportional, we can expect the linear relationship between SIF and GPP to hold. On the other hand, when the decrease in the two is not proportional, the linear relationship breaks down, resulting in a complex dynamic between GPP and SIF [Porcar-Castell et al., 2014].

The breakdown of the linear relationship is distinctly noticeable between sPRI and SIF yield (Figure 5), where all the three points deviate away from the fitted least squares line because of a drop in SIF yield. However, this pattern is not as strong for the SIF yield and LUE relationship. At Sturt Plains, throughout the range of APAR, both LUE and SIF yield show similar effects (Figure 8). In particular, after a certain maximum of APAR both LUE and SIF yield drop (points enclosed by rectangles in Figure 8 which also correspond to high ECI) partially preserving the linear relationship.

Leaf-level instantaneous relationship between fluorescence and photosynthesis tends to show nonlinear asymptotic behavior. Moreover, the parameters of this relationship such as the slope in linear regime, the point where nonlinearity starts to become significant, and the degree of departure from a linear relationship may vary across ecosystems [Damm et al., 2015]. However, our study shows that the relationship between SIF and GPP tends to remain linear at canopy scale under a range of conditions. Although, this facilitates empirical estimation of GPP based on SIF, it also highlights the fact that principal mechanisms operating at canopy scales are more complex than at a leaf scale.

Nonetheless, we cannot completely rule out the nonlinear effects of NPQ on the dynamics between SIF and GPP since at least one of the points with high ECI did show the tendency to move away from the fitted line (Figure 4). Previous studies have argued that APAR and LUE are the two main drivers of SIF [Yoshida et al., 2015].

However, the effect of NPQ on LUE and SIF are complex and we may not be able to adequately understand it unless we explicitly factor NPQ, in addition to APAR and LUE, in our analyses.

Open savanna grasslands play an important role in the regional biogeochemistry in Australia. Monitoring their GPP is important, but remote sensing-based models do not track GPP of these systems very well [Kanniah *et al.*, 2009]. We calibrated the MOD17 model at Sturt Plains using tower and MODIS data and found that it correlated poorly ($r < 0.4$) with tower GPP. Recent studies have attempted to model GPP using SIF as the only predictor in a simple linear relation at monthly time scales [Frankenberg *et al.*, 2011]. Efforts are also ongoing to use sPRI for tracking LUE. One of the key challenges in using sPRI for estimating LUE has been that the relationship changes from site to site, and hence, parameters calibrated at one location cannot be applied at other sites [Garbulsky *et al.*, 2011; Goerner *et al.*, 2011]. Following Figure 5, we can use sPRI and SIF yield to demarcate conditions when SIF and GPP are likely to be within a linear regime. Going further, we can also normalize SIF yield with sPRI, which resulted in an improved correlation with LUE. Cheng *et al.* [2013] showed similar improvement in GPP estimation using SIF (in red zone) and PRI in multiple linear regression framework. Damm *et al.* [2010] followed a light-use efficiency approach for modeling GPP and showed that combined SIF yield and PRI provides better estimates of LUE. Based on the data points available in this study, it is difficult to judge the wider applicability of this procedure, but future studies can examine if OCO-2 SIF and MODIS PRI can together provide better information of LUE than SIF alone.

PRI is sensitive to the structural and directional effects and is also responds to changes in pigment pools over seasonal time scale [Rahimzadeh-Bajgiran *et al.*, 2012]. However, in the morphologically simple very short (less than one meter) canopies at Sturt Plains structural effects such as mutual shading are likely to be small. In seasonal grasses leaf area development and biochemical development are tightly coupled. PROSAIL outputs also showed that LAI and leaf chlorophyll concentration developed and decayed almost synchronously (Figure 6) at Sturt Plains. Under such conditions, normalizing by EVI appears to be an effective approach that control for other effects on sPRI. It will be worth investigating if this approach works more widely in grasslands.

To understand how atmospheric constituents affect PRI, we atmospherically corrected MODIS data with the 6S [Verote *et al.*, 1997] model and calculated sPRI from the at-surface reflectance. We input mean parameters in 6S since the site-specific measurements of the relevant variables were not available. At-surface sPRI showed a relatively weaker correlation with LUE and SIF yield (results not shown).

OCO-2 records observations in the nadir and glint mode. In our analyses we did not notice a significant effect of view angle on the relationship between SIF and GPP. Other studies have also reported that SIF is not sensitive to the directional effects at low LAI [Koffi *et al.*, 2015].

The second objective of this study was to understand the accuracy of SIF predicted by the SCOPE model and assesses the capacity of the SCOPE model to constrain the estimates of V_{cmax} . SIF predicted by the SCOPE model matched the seasonality of OCO-2 SIF for the seven different values of V_{cmax} . However, the magnitude of the simulated SIF was consistently lower than the observed SIF. We employed the version 1.61 of the model where the fluorescence yield was set to 0.01 [Vilfan *et al.*, 2016], which appears to be low leading to a consistently negative bias in predicted SIF relative to the SIF observed by OCO-2. Note that in the version 1.53 of the model the yield parameter was set to 0.02, which in our case will reduce the negative bias and will provide more accurate estimates of SIF.

The ability of the SCOPE model to utilize OCO-2 SIF for constraining V_{cmax} was weak. In fact, predicted SIF showed little sensitivity to V_{cmax} and the agreement between the modeled and observed SIF was nearly the same for the V_{cmax} ranging from 10 to 180 $\mu\text{mol m}^{-2} \text{s}^{-1}$. A detailed analysis of why SCOPE is not able to constrain the estimates of V_{cmax} and thereby improve GPP predictions is beyond the scope of this study. Here we discuss some possibilities and offer a few hypotheses that future studies can investigate. The SCOPE model currently distinguishes between C3 and C4 photosynthesis, which is consistent with the knowledge of the fundamental processes. Although the models of leaf-level photosynthesis and its upscaling to canopy and ecosystem levels are well established, efforts to model the ecophysiological relationship amongst steady state solar-induced fluorescence, photosynthesis, and nonphotochemical quenching are in very early stages. SCOPE represents a significant first step forward in this direction. However, our current knowledge of the variability of fluorescence parameters such as the ratio of absorption cross section of photosystem (PS)

I and II, and the quantum efficiency of PS II is poor. Similarly, we do not have an adequate understanding of the relevant processes to build a model of nonphotochemical quenching based on theory. Fluorescence emission in the SCOPE model is parameterized based on a nonlinear relationship between the degree of light saturation and nonphotochemical decay [Tol *et al.*, 2014]. This nonlinear relationship is derived from limited data and the assumption that the empirical relationship is invariant and applies everywhere needs to be tested and may not be valid. Moreover, the actual degree of light saturation experienced by vegetation can vary between biomes and even between species because of the difference in sensitivity of ecophysiological processes to variables such as PAR, temperature, and vapor pressure deficit.

Modeling of integrated, canopy level SIF is also sensitive to how fluorescence emission travels through leaves and canopies including BRDF and reabsorption effects and the connection between SIF and GPP. Although SIF yield can be interpreted as directly related to electron transport rate (ETR) [Genty *et al.*, 1989], under certain environmental conditions the relationship between ETR and GPP can break down or become weak due to processes such as photorespiration, nitrogen metabolism, and the donation of electron to oxygen [Cervic *et al.*, 1996; Maxwell and Johnson, 2000]. A sensitivity analysis of SCOPE showed that the modeled SIF was not very sensitive to V_{cmax} [Koffi *et al.*, 2015]. In fact, SIF simulated by the SCOPE model is more sensitive to incoming PAR, VPD, temperature, LAI, atmospheric CO₂ concentration, and leaf chlorophyll concentration than V_{cmax} [Verrelst *et al.*, 2016]. Based on the sensitivity analyses, Verrelst *et al.* [2016] have suggested that together fluorescence in O₂-B (687 nm) and O₂-A (760 nm) bands provide the best constrain on the photosynthetic activity in the SCOPE model. Thus, a combination of these two bands is likely to lead to a better estimation of V_{cmax} by the SCOPE model. OCO-2 SIF does not include retrievals at 687 nm, and it is likely that SCOPE's ability to constrain V_{cmax} will improve if it is also constrained by SIF at 687 nm, in addition to 760 nm. Having observations in a number of wavelengths within the fluorescence range (680–800 nm) is also likely to provide better constraints on the model outputs. A new instrument, Chlorophyll Fluorescence Imaging Spectrometer (CFIS), developed at the Jet Propulsion Laboratory (JPL), covers a larger range of fluorescence spectrum and has started taking airborne measurements of SIF. In future studies we intend to use CFIS measurements to constrain the SCOPE simulation. We also need better understanding of how the leaf-level relationship between fluorescence and photosynthesis propagates and scales up from a leaf to canopy to ecosystem level. Relevant measurements that can diagnose the flow of energy along different pathways at a leaf and canopy scale will help us understand the role of NPQ in modulating the relationship between SIF and photosynthesis and will help us improve models. The Fluorescence Imaging Spectrometer (FLORIS) of the Fluorescence Explorer (FLEX) mission of the European Space Agency (ESA) will enable global mapping of SIF at a spatial resolution of 300 m with a revisit time of about 1 month. With a spectral range between 500 and 789 nm, it will cover the entire fluorescence spectrum including the wavelengths relevant for PRI. This will provide very useful data for modeling and inverting photosynthesis parameters using models such SCOPE.

5. Conclusion

Measurements of SIF from space have opened up the possibility of more accurate and reliable monitoring of GPP. However, the relationship amongst SIF, photosynthesis, and NPQ at the canopy level is not adequately understood. To successfully utilize SIF for modeling and monitoring GPP, we need a more mechanistic understanding of the relationship between SIF and GPP under different environmental conditions and develop models that can realistically simulate this relationship. In this study we examined the relationship of OCO-2 SIF with GPP and PRI at a well-characterized open savanna grassland site and also tested the potential of the SCOPE model to simulate SIF and optimize V_{cmax} . Given the complexities in interpreting PRI signal, we cannot positively conclude about the potential of MODIS PRI in elucidating the effect of NPQ on the relationship between SIF and GPP. Nonetheless, our analyses clearly show that despite a complex relationship between photosynthesis and fluorescence at a leaf level, the relationship between SIF and GPP at canopy scales remains robust under different environmental conditions in grassland. Our results thus strongly support the ongoing effort to utilize SIF for improved monitoring of GPP.

The SCOPE model represents an important innovation in linking SIF and GPP potentially allowing us to use SIF to recover parameters of photosynthesis. Although, the model captured the seasonality of SIF well, it was not able to constrain V_{cmax} . As pointed out in section 4, in part, this could be due to the nonoptimality of the

wavelengths at which SIF is measured by OCO-2. But, this might also suggest that the formalization that links SIF and GPP in the SCOPE model needs improvements. From the point of view of GPP estimation, using SIF alone or with sPRI in a simple linear relation appear to be a better approach than employing SIF to recover the parameters of photosynthesis models.

Acknowledgments

This research was carried out at the Jet Propulsion Laboratory, California Institute of Technology, under a contract with the National Aeronautics and Space Administration, Copyright 2017, California Institute of Technology. The authors would like to acknowledge support and funding from OzFlux and the overarching Terrestrial Ecosystem Research Network (TERN), which is supported by the Australian Government through the National Collaborative Research Infrastructure Strategy. This work utilized data collected by grants funded by the Australian Research Council (DP0344744, DP0772981, and DP130101566). Beringer is funded under an ARC FT (FT110100602). Data presented in this paper are included in the supporting information. The two models, PROSAIL and SCOPE, are open source and are available free. PROSAIL can be downloaded from <http://teledetection.ipgp.jussieu.fr/prosail/>, and SCOPE can be obtained from <https://github.com/Christiaanvandertol/SCOPE>.

References

- Anand, S. (1994), Human Development Index: Methodology and measurement Rep., Human Development Report Office (HDRO), United Nations Development Programme (UNDP).
- Anand, S., and A. Sen (2000), The income component of the Human Development Index, *J. Hum. Dev.*, 1(1), 83–106.
- Baker, N., and K. Hardwick (1973), Biochemical and physiological aspects of leaf development in cocoa (*Theobroma cacao*): I. Development of chlorophyll and photosynthetic activity, *New Phytol.*, 72(6), 1315–1324.
- Baker, N. R. (2008), Chlorophyll fluorescence: A probe of photosynthesis in vivo, *Annu. Rev. Plant Biol.*, 59(1), 89–113, doi:10.1146/annurev.arplant.59.032607.092759.
- Beringer, J., J. Hacker, L. B. Hutley, R. Leuning, S. K. Arndt, R. Amiri, L. Bannehr, L. A. Cernusak, S. Grover, and C. Hensley (2011a), Special-savanna patterns of energy and carbon integrated across the landscape, *Bull. Am. Meteorol. Soc.*, 92(11), 1467.
- Beringer, J., L. B. Hutley, J. M. Hacker, and B. Neininger (2011b), Patterns and processes of carbon, water and energy cycles across northern Australian landscapes: From point to region, *Agric. For. Meteorol.*, 151(11), 1409–1416.
- Beringer, J., et al. (2016), An introduction to the Australian and New Zealand flux tower network—OzFlux, *Biogeosci. Discuss.*, 2016, 1–52, doi:10.5194/bg-2016-152.
- Butler, W. L. (1978), Energy distribution in the photochemical apparatus of photosynthesis, *Annu. Rev. Plant Physiol.*, 29(1), 345–378.
- Cerovic, Z., Y. Goulas, M. Gorbunov, J.-M. Briantais, L. Camenen, and I. Moya (1996), Fluorescence of water stress in plants: Diurnal changes of the mean lifetime and yield of chlorophyll fluorescence, measured simultaneously and at distance with a τ -LIDAR and a modified PAM-fluorimeter, in maize, sugar beet, and Kalanchoë, *Remote Sens. Environ.*, 58(3), 311–321.
- Cheng, Y.-B., E. Middleton, Q. Zhang, K. Huemmrich, P. Campbell, L. Corp, B. Cook, W. Kustas, and C. Daughtry (2013), Integrating solar induced fluorescence and the photochemical reflectance index for estimating gross primary production in a cornfield, *Remote Sens. (Basel)*, 5(12), 6857–6879, doi:10.3390/rs5126857.
- Crisp, D., et al. (2004), The Orbiting Carbon Observatory (OCO) mission, *Adv. Space Res.*, 34(4), 700–709, doi:10.1016/j.asr.2003.08.062.
- Damm, A., et al. (2010), Remote sensing of sun-induced fluorescence to improve modeling of diurnal courses of gross primary production (GPP), *Global Change Biol.*, 16(1), 171–186, doi:10.1111/j.1365-2486.2009.01908.x.
- Damm, A., L. Guanter, E. Paul-Limoges, C. Van der Tol, A. Hueni, N. Buchmann, W. Eugster, C. Ammann, and M. Schaepman (2015), Far-red sun-induced chlorophyll fluorescence shows ecosystem-specific relationships to gross primary production: An assessment based on observational and modeling approaches, *Remote Sens. Environ.*, 166, 91–105.
- Darvishzadeh, R., A. Skidmore, M. Schlerf, and C. Atzberger (2008), Inversion of a radiative transfer model for estimating vegetation LAI and chlorophyll in a heterogeneous grassland, *Remote Sens. Environ.*, 112(5), 2592–2604, doi:10.1016/j.rse.2007.12.003.
- Demmig-Adams, B., and W. W. Adams III (1996), Xanthophyll cycle and light stress in nature: Uniform response to excess direct sunlight among higher plant species, *Planta*, 198(3), 460–470.
- Drolet, G., E. Middleton, K. Huemmrich, F. Hall, B. Amiro, A. Barr, T. Black, J. McCaughey, and H. Margolis (2008), Regional mapping of gross light-use efficiency using MODIS spectral indices, *Remote Sens. Environ.*, 112(6), 3064–3078.
- Feret, J.-B., C. François, G. P. Asner, A. A. Gitelson, R. E. Martin, L. P. Bidel, S. L. Ustin, G. le Maire, and S. Jacquemoud (2008), PROSPECT-4 and 5: Advances in the leaf optical properties model separating photosynthetic pigments, *Remote Sens. Environ.*, 112(6), 3030–3043.
- Filella, I., A. Porcar-Castell, S. Munñé-Bosch, J. Bäck, M. Garbulska, and J. Peñuelas (2009), PRI assessment of long-term changes in carotenoids/chlorophyll ratio and short-term changes in de-epoxidation state of the xanthophyll cycle, *Int. J. Remote Sens.*, 30(17), 4443–4455.
- Flexas, J., and H. Medrano (2002), Drought-inhibition of photosynthesis in C3 plants: Stomatal and non-stomatal limitations revisited, *Ann. Bot.*, 89(2), 183–189.
- Fox, I., V. Neldner, G. Wilson, and P. Bannink (2001), *The Vegetation of the Tropical Australian Savannas*, Environmental Protection Agency, Brisbane.
- Frankenberg, C., J. B. Fisher, J. Worden, G. Badgley, S. S. Saatchi, J. E. Lee, G. C. Toon, A. Butz, M. Jung, and A. Kuze (2011), New global observations of the terrestrial carbon cycle from GOSAT: Patterns of plant fluorescence with gross primary productivity, *Geophys. Res. Lett.*, 38, L17706, doi:10.1029/2011GL048738.
- Frankenberg, C., C. O'Dell, L. Guanter, and J. McDuffie (2012), Remote sensing of near-infrared chlorophyll fluorescence from space in scattering atmospheres: Implications for its retrieval and interferences with atmospheric CO₂ retrievals, *Atmos. Meas. Tech.*, 5(8), 2081–2094.
- Frankenberg, C., C. O'Dell, J. Berry, L. Guanter, J. Joiner, P. Köhler, R. Pollock, and T. E. Taylor (2014), Prospects for chlorophyll fluorescence remote sensing from the Orbiting Carbon Observatory-2, *Remote Sens. Environ.*, 147, 1–12.
- Frankenberg, C., R. Pollock, R. Lee, R. Rosenberg, J.-F. Blavier, D. Crisp, C. O'Dell, G. Osterman, C. Roehl, and P. Wennberg (2015), The Orbiting Carbon Observatory (OCO-2): Spectrometer performance evaluation using pre-launch direct sun measurements, *Atmos. Meas. Tech.*, 8(1), 301–313.
- Gamon, J. A., and J. A. Berry (2012), Facultative and constitutive pigment effects on the photochemical reflectance index (PRI) in Sun and shade conifer needles, *Isr. J. Plant Sci.*, 60(1–2), 85–95.
- Gamon, J. A., K. F. Huemmrich, C. Y. Wong, I. Ensminger, S. Garrity, D. Y. Hollinger, A. Noormets, and J. Penuelas (2016), A remotely sensed pigment index reveals photosynthetic phenology in evergreen conifers, *Proc. Natl. Acad. Sci. U.S.A.*, 113(46), 13,087–13,092, doi:10.1073/pnas.1606162113.
- Gamon, J., J. Penuelas, and C. Field (1992), A narrow-waveband spectral index that tracks diurnal changes in photosynthetic efficiency, *Remote Sens. Environ.*, 41(1), 35–44.
- Garbulska, M. F., J. Peñuelas, J. Gamon, Y. Inoue, and I. Filella (2011), The photochemical reflectance index (PRI) and the remote sensing of leaf, canopy and ecosystem radiation use efficiencies: A review and meta-analysis, *Remote Sens. Environ.*, 115(2), 281–297.
- Garrity, S. R., J. U. Eitel, and L. A. Vierling (2011), Disentangling the relationships between plant pigments and the photochemical reflectance index reveals a new approach for remote estimation of carotenoid content, *Remote Sens. Environ.*, 115(2), 628–635.

- Genty, B., J.-M. Briantais, and N. R. Baker (1989), The relationship between the quantum yield of photosynthetic electron transport and quenching of chlorophyll fluorescence, *Biochim. Biophys. Acta Gen. Subj.*, *990*(1), 87–92, doi:10.1016/S0304-4165(89)80016-9.
- Glenn, E. P., A. R. Huete, P. L. Nagler, and S. G. Nelson (2008), Relationship between remotely-sensed vegetation indices, canopy attributes and plant physiological processes: What vegetation indices can and cannot tell us about the landscape, *Sensors*, *8*(4), 2136–2160.
- Goerner, A., M. Reichstein, E. Tomelleri, N. Hanan, S. Rambal, D. Papale, D. Dragoni, and C. Schmullius (2011), Remote sensing of ecosystem light use efficiency with MODIS-based PRI, *Biogeosciences*, *8*(1), 189–202.
- Govindjee, J. Barber, W. A. Cramer, J. H. C. Goedheer, J. Lavorel, R. Marcelle, and B. Zilinskas (Eds.) (1987), *Excitation Energy and Electron Transfer in Photosynthesis, Dedicated to Warren L. Butler*, 388 pp., Springer/Martinus Nijhoff, Netherlands.
- Guan, K., J. Berry, Y. Zhang, J. Joiner, L. Guanter, G. Badgley, and D. B. Lobell (2015), Improving the monitoring of crop productivity using spaceborne solar-induced fluorescence, *Global Change Biol.*, *22*, 716–726, doi:10.1111/gcb.13136.
- Guanter, L., C. Frankenberg, A. Dudhia, P. E. Lewis, J. Gómez-Dans, A. Kuze, H. Suto, and R. G. Grainger (2012), Retrieval and global assessment of terrestrial chlorophyll fluorescence from GOSAT space measurements, *Remote Sens. Environ.*, *121*, 236–251.
- Hall, F. G., T. Hilker, N. C. Coops, A. Lyapustin, K. F. Huemmrich, E. Middleton, H. Margolis, G. Drolet, and T. A. Black (2008), Multi-angle remote sensing of forest light use efficiency by observing PRI variation with canopy shadow fraction, *Remote Sens. Environ.*, *112*(7), 3201–3211.
- Hammerling, D. M., A. M. Michalak, and S. R. Kawa (2012), Mapping of CO₂ at high spatiotemporal resolution using satellite observations: Global distributions from OCO-2, *J. Geophys. Res.*, *117*, D06306, doi:10.1029/2011JD017015.
- Heimann, M., and M. Reichstein (2008), Terrestrial ecosystem carbon dynamics and climate feedbacks, *Nature*, *451*(7176), 289–292, doi:10.1038/nature06591.
- Hilker, T., A. Lyapustin, F. G. Hall, Y. Wang, N. C. Coops, G. Drolet, and T. A. Black (2009), An assessment of photosynthetic light use efficiency from space: Modeling the atmospheric and directional impacts on PRI reflectance, *Remote Sens. Environ.*, *113*(11), 2463–2475, doi:10.1016/j.rse.2009.07.012.
- Hutley, L. B., J. Beringer, P. R. Isaac, J. M. Hacker, and L. A. Cernusak (2011), A sub-continental scale living laboratory: Spatial patterns of savanna vegetation over a rainfall gradient in northern Australia, *Agric. For. Meteorol.*, *151*(11), 1417–1428, doi:10.1016/j.agrformet.2011.03.002.
- Jacquemoud, S., and F. Baret (1990), PROSPECT: A model of leaf optical properties spectra, *Remote Sens. Environ.*, *34*(2), 75–91.
- Jacquemoud, S., W. Verhoef, F. Baret, C. Bacour, P. J. Zarco-Tejada, G. P. Asner, C. François, and S. L. Ustin (2009), PROSPECT + SAIL models: A review of use for vegetation characterization, *Remote Sens. Environ.*, *113*, S56–S66, doi:10.1016/j.rse.2008.01.026.
- Joiner, J., Y. Yoshida, A. Vasilkov, K. Schaefer, M. Jung, L. Guanter, Y. Zhang, S. Garrity, E. Middleton, and K. Huemmrich (2014), The seasonal cycle of satellite chlorophyll fluorescence observations and its relationship to vegetation phenology and ecosystem atmosphere carbon exchange, *Remote Sens. Environ.*, *152*, 375–391.
- Jung, M., et al. (2011), Global patterns of land-atmosphere fluxes of carbon dioxide, latent heat, and sensible heat derived from eddy covariance, satellite, and meteorological observations, *J. Geophys. Res.*, *116*, G00J07, doi:10.1029/2010JG001566.
- Kanniah, K. D., J. Beringer, P. North, and L. Hutley (2012), Control of atmospheric particles on diffuse radiation and terrestrial plant productivity: A review, *Prog. Phys. Geogr.*, *36*(2), 209–237.
- Kanniah, K., J. Beringer, L. Hutley, N. Tapper, and X. Zhu (2009), Evaluation of collections 4 and 5 of the MODIS gross primary productivity product and algorithm improvement at a tropical savanna site in northern Australia, *Remote Sens. Environ.*, *113*(9), 1808–1822.
- Keenan, T., I. Baker, A. Barr, P. Ciais, K. Davis, M. Dietze, D. Dragoni, C. M. Gough, R. Grant, and D. Hollinger (2012), Terrestrial biosphere model performance for inter-annual variability of land-atmosphere CO₂ exchange, *Global Change Biol.*, *18*(6), 1971–1987.
- Knyazikhin, Y., J. Martonchik, R. Myneni, D. Diner, and S. Running (1998), Synergistic algorithm for estimating vegetation canopy leaf area index and fraction of absorbed photosynthetically active radiation from MODIS and MISR data, *J. Geophys. Res.*, *103*(D24), 32,257–32,275, doi:10.1029/98JD02462.
- Koffi, E. N., P. J. Rayner, A. J. Norton, C. Frankenberg, and M. Scholze (2015), Investigating the usefulness of satellite-derived fluorescence data in inferring gross primary productivity within the carbon cycle data assimilation system, *Biogeosciences*, *12*(13), 4067–4084, doi:10.5194/bg-12-4067-2015.
- Krause, G., and E. Weis (1991), Chlorophyll fluorescence and photosynthesis: The basics, *Annu. Rev. Plant Biol.*, *42*(1), 313–349.
- Lee, J.-E., J. A. Berry, C. van der Tol, X. Yang, L. Guanter, A. Damm, I. Baker, and C. Frankenberg (2015), Simulations of chlorophyll fluorescence incorporated into the Community Land Model version 4, *Global Change Biol.*, *21*(9), 3469–3477, doi:10.1111/gcb.12948.
- Magney, T. S., L. A. Vierling, J. U. Eitel, D. R. Huggins, and S. R. Garrity (2016), Response of high frequency photochemical reflectance index (PRI) measurements to environmental conditions in wheat, *Remote Sens. Environ.*, *173*, 84–97.
- Mahadevan, P., S. C. Wofsy, D. M. Matross, X. Xiao, A. L. Dunn, J. C. Lin, C. Gerbig, J. W. Munger, V. Y. Chow, and E. W. Gottlieb (2008), A satellite-based biosphere parameterization for net ecosystem CO₂ exchange: Vegetation Photosynthesis and Respiration Model (VPRM), *Global Biogeochem. Cycles*, *22*, B2005, doi:10.1029/2006GB002735.
- Maxwell, K., and G. N. Johnson (2000), Chlorophyll fluorescence—a practical guide, *J. Exp. Bot.*, *51*(345), 659–668.
- Mohammed, G. H., Y. Goulas, F. Magnani, J. Moreno, J. Olejníčková, U. Rascher, C. van der Tol, W. Verhoef, A. Ač, and F. Daumard (2014), 2012 FLEX/Sentinel-3 Tandem Mission Photosynthesis Study, in Final report. ESTEC contract no. 4000106396/12/NL/AF.
- Mu, Q., M. Zhao, and S. W. Running (2011), Improvements to a MODIS global terrestrial evapotranspiration algorithm, *Remote Sens. Environ.*, *115*(8), 1781–1800.
- Müller, P., X.-P. Li, and K. K. Niyogi (2001), Non-photochemical quenching. A response to excess light energy, *Plant Physiol.*, *125*(4), 1558–1566, doi:10.1104/pp.125.4.1558.
- Plascyk, J. A., and F. C. Gabriel (1975), The Fraunhofer line discriminator MKII—An airborne instrument for precise and standardized ecological luminescence measurement, *IEEE Trans. Instrum. Meas.*, *24*(4), 306–313.
- Porcar-Castell, A., E. Tyystjärvi, J. Atherton, C. van der Tol, J. Flexas, E. E. Pfundel, J. Moreno, C. Frankenberg, and J. A. Berry (2014), Linking chlorophyll a fluorescence to photosynthesis for remote sensing applications: Mechanisms and challenges, *J. Exp. Bot.*, *65*(15), 4065–4095, doi:10.1093/jxb/eru191.
- Rahimzadeh-Bajgiran, P., M. Munehiro, and K. Omasa (2012), Relationships between the photochemical reflectance index (PRI) and chlorophyll fluorescence parameters and plant pigment indices at different leaf growth stages, *Photosynth. Res.*, *113*(1–3), 261–271, doi:10.1007/s1120-012-9747-4.
- Renger, G. (2007), Chapter 1. Overview of primary processes of photosynthesis, *Prim. Process. Photosynth.*, *8*, 5–35, doi:10.1039/9781847558152-00001.
- Running, S. W., R. R. Nemani, F. A. Heinsch, M. Zhao, M. Reeves, and H. Hashimoto (2004), A continuous satellite-derived measure of global terrestrial primary production, *BioScience*, *54*(6), 547–560, doi:10.1641/0006-3568(2004)054[0547:acsmog]2.0.co;2.
- Schaaf, C., F. Gao, A. Strahler, W. Lucht, X. Li, T. Tsang, N. Strugnell, X. Zhang, Y. Jin, and J.-P. Muller (2002), First operational BRDF, albedo nadir reflectance products from MODIS, *Remote Sens. Environ.*, *83*(1), 135–148.

- Schimel, D., R. Pavlick, J. B. Fisher, G. P. Asner, S. Saatchi, P. Townsend, C. Miller, C. Frankenberg, K. Hibbard, and P. Cox (2015), Observing terrestrial ecosystems and the carbon cycle from space, *Global Change Biol.*, *21*(5), 1762–1776, doi:10.1111/gcb.12822.
- Sims, D. A., and J. A. Gamon (2002), Relationships between leaf pigment content and spectral reflectance across a wide range of species, leaf structures and developmental stages, *Remote Sens. Environ.*, *81*(2), 337–354.
- Tol, C., J. Berry, P. Campbell, and U. Rascher (2014), Models of fluorescence and photosynthesis for interpreting measurements of solar-induced chlorophyll fluorescence, *J. Geophys. Res. Biogeosci.*, *119*, 2312–2327, doi:10.1002/2014JG002713.
- Tol, V. D. C., W. Verhoef, J. Timmermans, A. Verhoef, and Z. Su (2009), An integrated model of soil-canopy spectral radiances, photosynthesis, fluorescence, temperature and energy balance, *Biogeosciences*, *6*(12), 3109–3129.
- Vasilkov, A., J. Joiner, and R. Spurr (2013), Note on rotational-Raman scattering in the O₂ A- and B-bands, *Atmos. Meas. Tech.*, *6*(4), 981–990, doi:10.5194/amt-6-981-2013.
- Verhoef, W. (1984), Light scattering by leaf layers with application to canopy reflectance modeling: The SAIL model, *Remote Sens. Environ.*, *16*(2), 125–141, doi:10.1016/0034-4257(84)90057-9.
- Verma, M., et al. (2015), Improving the performance of remote sensing models for capturing intra- and inter-annual variations in daily GPP: An analysis using global FLUXNET tower data, *Agric. For. Meteorol.*, *214–215*, 416–429, doi:10.1016/j.agrformet.2015.09.005.
- Vermote, E. F., D. Tanré, J. L. Deuze, M. Herman, and J.-J. Morcette (1997), Second simulation of the satellite signal in the solar spectrum, 6S: An overview, *IEEE Trans. Geosci. Remote Sens.*, *35*(3), 675–686.
- Verrelst, J., J. P. Rivera, C. van der Tol, F. Magnani, G. Mohammed, and J. Moreno (2015), Global sensitivity analysis of the SCOPE model: What drives simulated canopy-leaving sun-induced fluorescence?, *Remote Sens. Environ.*, *166*, 8–21, doi:10.1016/j.rse.2015.06.002.
- Verrelst, J., C. van der Tol, F. Magnani, N. Sabater, J. P. Rivera, G. Mohammed, and J. Moreno (2016), Evaluating the predictive power of Sun-induced chlorophyll fluorescence to estimate net photosynthesis of vegetation canopies: A SCOPE modeling study, *Remote Sens. Environ.*, *176*, 139–151, doi:10.1016/j.rse.2016.01.018.
- Vilfan, N., C. van der Tol, O. Muller, U. Rascher, and W. Verhoef (2016), Fluspect-B: A model for leaf fluorescence, reflectance and transmittance spectra, *Remote Sens. Environ.*, *186*, 596–615.
- Xiao, X., Q. Zhang, B. Braswell, S. Urbanski, S. Boles, S. Wofsy, B. Moore III, and D. Ojima (2004), Modeling gross primary production of temperate deciduous broadleaf forest using satellite images and climate data, *Remote Sens. Environ.*, *91*(2), 256–270.
- Yoshida, Y., J. Joiner, C. Tucker, J. Berry, J. E. Lee, G. Walker, R. Reichle, R. Koster, A. Lyapustin, and Y. Wang (2015), The 2010 Russian drought impact on satellite measurements of solar-induced chlorophyll fluorescence: Insights from modeling and comparisons with parameters derived from satellite reflectances, *Remote Sens. Environ.*, *166*, 163–177, doi:10.1016/j.rse.2015.06.008.
- Zarco-Tejada, P. J., V. González-Dugo, L. Williams, L. Suárez, J. A. Berni, D. Goldhamer, and E. Fereres (2013), A PRI-based water stress index combining structural and chlorophyll effects: Assessment using diurnal narrow-band airborne imagery and the CWSI thermal index, *Remote Sens. Environ.*, *138*, 38–50.
- Zhang, Q., X. Xiao, B. Braswell, E. Linder, F. Baret, and B. Moore (2005), Estimating light absorption by chlorophyll, leaf and canopy in a deciduous broadleaf forest, using MODIS data and a radiative transfer model, *Remote Sens. Environ.*, *99*, 357–371.
- Zhang, Y., L. Guanter, J. A. Berry, J. Joiner, C. van der Tol, A. Huete, A. Gitelson, M. Voigt, and P. Kohler (2014), Estimation of vegetation photosynthetic capacity from space-based measurements of chlorophyll fluorescence for terrestrial biosphere models, *Global Change Biol.*, *20*(12), 3727–3742, doi:10.1111/gcb.12664.